

Effect of sintering temperature on performance and durability of HT-PEFC cathodes

G. Borisov^{1*}, S. Avramov¹, E. Petkucheva¹, E. Lefterova¹, E. Slavcheva¹, W. Lehnert²

¹ Acad. E. Budevski Institute of Electrochemistry and Energy Systems, Bulgarian Academy of Sciences, 10 Acad. G. Bonchev St., Sofia 1113, Bulgaria

² Institute of Energy and Climate Research (IEK-3), Forschungszentrum Jülich GmbH, Germany

Received March 10, 2017 Revised March 30, 2017

The design of the electrodes applicable for high temperature PEM fuel cells (HTPEFC) is a delicate balancing of the transport media. The conductivity of gases, electrons, and protons must be optimized in order to provide efficient transport to and from the electrochemical active area. This article presents the effects of heat treatment on the properties of the anode gas diffusion electrode integrated in a membrane electrode assembly (MEA) with phosphoric acid doped poly-benzimidazol membrane. The sintering procedure reflects on the catalyst activity as well as on the stability and durability of the electrode. The electrochemical performance of the cell was investigated by steady state polarization curves, potential-dynamic curves and electrochemical impedance spectroscopy. It was found, that the different pore size distribution in the active catalytic layer treated at different temperatures affects the transport limitations of the reaction. The optimal cell performance is established for the electrode sintered at 340°C. The measured degradation rate is close to 0.001 μ V/h.

Key words: PEM fuel cell, degradation, catalysts, HT-PEFC cathodes.

INTRODUCTION

The high-temperature polymer electrolyte fuel cell (HT-PEFC) is a chemical to electrical energy converting electrochemical system operating in the temperature range 160 - 200°C. It offers a number of advantages compared to the low temperature Nafion®-based PEMFC operating at 80-90 °C [1-3]. First of all, the higher operating temperature improves the kinetics and increases the exchange current density of both hydrogen oxidation (HOR) and oxygen reduction (ORR) reactions. Secondly, there is no need for complex water management which makes the electrochemical system much simpler. Furthermore, HT-PEFC has a much higher CO tolerance and can work with reformat gas, particularly when middle distillates (kerosene, diesel, heating oil) are used to provide the necessary hydrogen. Therefore, HT-PEFC is considered as the next generation alternative power supply in ships, trains, buses, and other transport and stationary applications [4-6]. The electrolytes used in HT-PEMFC are mainly PBI-based (poly-benzimidazol) or hydride PBI-based polymers, which are capable to withstand the high operative temperatures [7]. In addition to the thermal stability, the PBI membranes exhibit excellent oxidative stability and mechanical flexibility. However, to achieve high proton conductivity,

these membranes have to be doped with concentrated phosphoric acid. The level of membrane doping and the MEA assembling procedure are of key importance for the efficient functioning of the whole fuel cell system [8-10]. Until now, the achieved level of phosphoric acid inside the membrane is around 400 wt. % which provides excellent proton conductivity (0.05S.cm⁻¹) and low crossover of the reactant gases. Nevertheless, the HT-PEFC performance is still lower compared with the LT PEMFC. The main reason is that the liquid phosphoric acid impedes the transport of the gaseous reagents and thus, the electrochemical reactions, due to the low solubility of oxygen in phosphoric acid and adsorption of the phosphate anions on the catalyst (Pt) surface. Another major problem in HT-PEFC is the leakage of the phosphoric acid out of the membrane which increases the resistance of the polymer electrolyte, causes corrosion problems, and decreases the cell energy efficiency [11-13]. In order to prevent these detrimental phenomena, a delicate balance between the gas delivery management, electron flow, and proton conductivity must be achieved, providing an efficient transport to and from the electrochemical reaction zone without degradation of the electrodes. This is accomplished through careful consideration of the gas diffusion electrode (GDE) architecture - catalytic layer, gas diffusion layer, and the distribution of the respective conducting network.

The HT-PEFC gas diffusion electrodes have a rather complex structure. The mechanical stability, electrical conductivity and gas delivery are

To whom all correspondence should be sent:
E-mail: gal.rusev@iees.bas.bg

provided by the gas diffusion layer (GDL), usually water proved carbon paper, while the gas distribution is controlled mainly by the top microporous layer (MPL) built from electro-conductive carbon material with high surface area and a hydrophobic polymer. On the top of MPL layer a catalytic layer (CL) is spread out which beside the carbon supported catalyst contains also a proper binding material. An optimal catalyst to binder ratio is required to ensure the integrity of the CL and achieve large triple phase boundary for the proceeding of the partial electrode reactions which in turn, improves both performance and catalyst utilization during the fuel cell operation [14-18]. The size and distribution of the pores in the catalytic layer also play a role for stability and durability of the electrodes and thus, for the service life of the HT-PEFC [11]. To keep the phosphoric acid inside the polymer membrane and far away from the produced water, the binders usually are highly hydrophilic polymers such as polybenzimidazol (PBI) [18-20], polytetrafluoroethylene (PTFE) [21-22], polyvinylidene difluoride (PVDF) [23-25]. In order to obtain catalytic layer with homogeneous pore distribution, excellent mass transport and increased area of the reactive zone (the triple-phase boundary), the GDEs before assembling have to be treated thermally (sintered) at temperatures close to the melting point of the used binding material. The exact temperature and the time of the sintering affect strongly the pore distribution and hydrophobicity of the electrode. In the literature there are only few papers dealing with the dependence of HT-PEFC performance durability on the parameters of the electrode thermal pretreatment. Some authors (MinJoong and Ai Suzuki), [24] reported that a benign thermal pretreatment of GDE electrodes at 150°C, aiming only at evaporation of the organic solvent used for the preparation of the catalytic ink, improves the cell performance. Kim et al. [26] showed that the GDL sintering in the temperature range 300-350°C improves the cell performance, while at more elevated temperatures it drops back down.

The objective of this work is to study in details the influence of the sintering temperature on the micro-pores size and distribution in HT-PEFC cathode containing polytetrafluoroethylene binder in the catalytic layer, and to elucidate the resulting effects on the electrode active surface area, cell efficiency and durability.

EXPERIMENTAL

The GDEs under study consisted of commercial gas diffusion layer with microspores layer on top

(H2315, Freudenberg) and a laboratory prepared catalytic layer with $1\text{mg}_{\text{Pt}}\cdot\text{cm}^{-2}$ loading, spread on the GDL using a “Doctor Blade” technique. The measured thickness of the as-prepared GDEs was about 40 μm and the geometric area - 14,44 cm^2 . The catalytic ink was prepared by ultrasonic horn and contained a mixture of carbon supported Pt (HiSpectm Fuel cell catalysts - 2000) and PTFE binder (commercial polymer suspension, Daneontm TFM 1700 PTFE). The prepared electrodes were sintered for 30 min at different ramp temperature (320, 340, 360°C), reached gradually with increment of 5 °C per min. The phase composition, surface structure, and morphology of the catalytic layers were investigated post mortem by X-ray diffraction (XRD, X-ray diffractometer Philips APD15). The diffraction data were collected at a constant rate of $0.02^{\circ}\text{s}^{-1}$ over an angle range of $2\theta = 10 - 90$ degrees. The size of Pt crystallites was determined by Scherrer equation [27]. The thermal behavior was investigated by TG_DTA and DSC methods using TA Instruments SDT 2960 Simultaneous DTA-TGA/DSC-TGA and DSC Q1000 (V9.9 Build 303). The measurements were carried out in the temperature range 0 – 400°C with Nitrogen as purge gas. In TG/DTA experiments a heating rate of 2 K/min was used, while in DSC measurements 10 fold higher (20K/min) heating/cooling rate was applied in order to increase the sensitivity.

The sintered electrodes were integrated in membrane electrode assemblies (MEA) using AB-PBI membrane (FuMA-Tech) and commercial cathodes (Pt/XC72). The AB-PBI membrane was doped with phosphoric acid following the procedure described in [25]. The doping level was 400 wt. % and the membrane thickness - 100 μm . The performance of thus prepared MEA was investigated in a HT-PEFC single cell at 160°C. The reagent gasses feeding the anode and cathode compartments were pure hydrogen and air at ambient pressure and flow rates corresponding to the stoichiometric factor cathode/anode 2/2. The MEA was run at $j=200\text{ mA}\cdot\text{cm}^{-2}$. The galvanostatic experiments were interrupted once at every 24 hours (break-in procedure) to record a control cathode polarization curve (again in galvanostatic mode with current increment of $50\text{ mA}\cdot\text{cm}^{-2}$) and an impedance spectrum in the frequency range of 100 MHz–100 kHz applying an AC voltage with amplitude of 5 mV. In order to evaluate the anode stability, the method of cyclic voltammetry was used as the cathode side of the cell was shunted, replacing the hydrogen by inert gas in order to prevent degradation of the catalytic layer. The CV

curves were recorded at potential scan rate of $50 \text{ mV}\cdot\text{s}^{-1}$ in the range (50mV to 500 mV).

RESULTS AND DISCUSSION

Figure 1 presents DSC curves of gas diffusion electrode (GDE) consisting of commercial gas diffusion layer (GDL) H2315 and a top laboratory prepared catalytic layer (CL) in which a carbon-dispersed Pt catalyst ($0.2 \text{ mg}\cdot\text{cm}^{-2}$) is mixed with 40% PTFE binder to obtain a catalytic ink spread on the GDL using a “Doctor Blade” technique. During DSC analysis the temperature is scanned in the range $0\text{-}400^\circ\text{C}$.

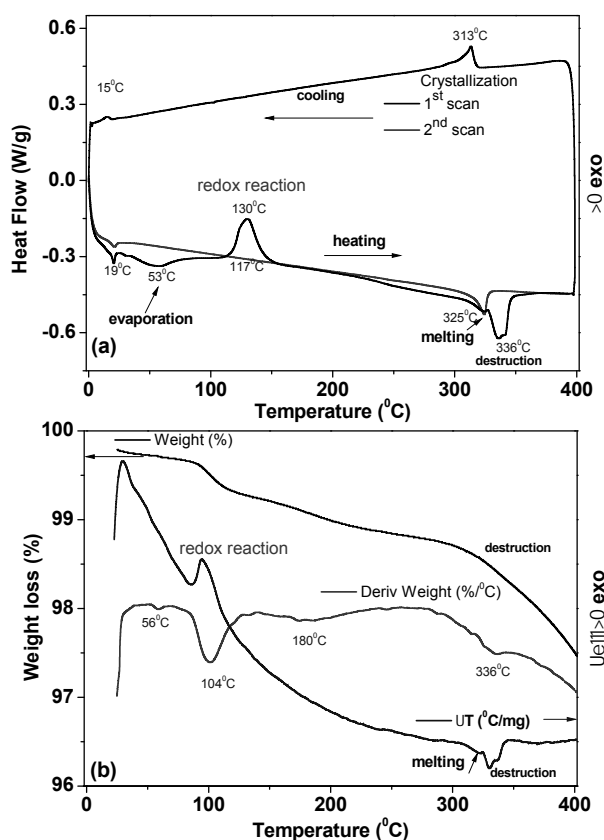


Fig. 1. DSCs: (a) and TG/DTG/DTA; (b) curves of the GDE under study.

In the first heating scan three endothermic and one endothermic peaks are registered (at 19, 53, 325-336, and 130°C , respectively). During the cooling scan only two exothermic peaks appeared (at 313 and 15°C) corresponding to the first and last exothermic peaks (at 19 and $325\text{-}336^\circ\text{C}$). These two peaks are reversible since they appear also during the second heating scan (in red). The first reversible peak (that at 19°C) is due to the PTFE polymorphous transition, while the one with doublet shape (at $325\text{-}336^\circ\text{C}$) is related to the phase transformations of PTFE. According to some

authors the observed doublet shape is due to the non-homogeneity of the PTFE in the CL [28]. Another reason could be consecutive processes of PTFE melting and destruction. The endothermic peak at 54°C is connected with evaporation of the alcohol remains in the microspores of CL. The irreversible exothermic peak observed at 130°C most probably is due to oxidative destruction since it proceeds with loss of weight. Such a process is also registered on TG/DTG/DTA curves (Fig. 1b), although there the peak appears at somehow lower temperature, which is due to the applied tenfold lower heating rate. The weight lost registered on the TG curve in the range $320\text{-}340^\circ\text{C}$ implies a superposition of PTFE melting and destruction processes, which might lead to changes in the porosity of CL and MPL of the GDE.

In order to check this assumption, the porosity of the catalytic layer before and after sintering at different temperatures (320 , 340 , and 360°C) is studied by standard porosimetry (Fig.2).

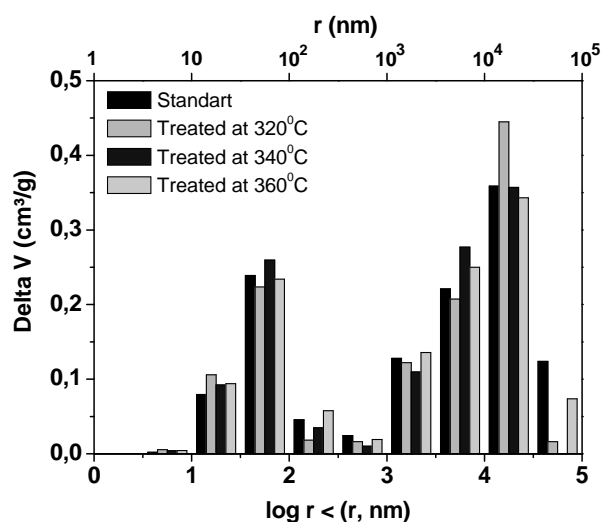


Fig. 2. Pore size distribution in CL of GDEs under study.

It is found that the sample treated at 320°C has a prevailing number of pores with size around $10\text{-}50 \mu\text{m}$, in similarity to the non-treated electrode. In contrast, for the samples treated at higher temperature than the PTFE melting point, the size of the pores varies in a very broad range – from 10 nm to $100 \mu\text{m}$, although the majority of the pores are grouped in two main groups – nanopores with size in the range $10\text{-}100 \text{ nm}$ and micropores with size $1\text{-}5 \mu\text{m}$. It can be assumed that the formation of the non-sized group of pores is related to destruction of the PTFE at higher temperatures.

The surface area of the as prepared and sintered electrodes was measured by BET analysis. The results obtained are presented in Table 1. They show a clear trend for decrease of the surface area

with increasing the sintering temperature. The difference between the nontreated electrode and that sintered at 320 °C (21.0 and 17.9 m².g⁻¹, respectively) is the biggest one.

Table 1. Influence of sintering temperature on the GDE surface area.

Temperature, °C	Surface area, m ² .g ⁻¹
as prepared	21.0
320	17.9
340	16.1
360	15.7

The GDE sintered at different temperatures were integrated as cathodes in MEA with a phosphoric acid doped PBI membrane against a self-made anode (Pt/XC72R) and tested in HT-PEFC single cell. The measured open circuit voltages were similar for all investigated samples - approximately 0.95V at 160 °C.

The performance tests were carried out in a galvanostatic mode at constant load of 0.2 A.cm⁻². In order to follow the occurring degradation phenomena, every 24 hours the performance tests were interrupted to record a control polarization curve and an impedance spectrum. Figure 4 presents the *E/j* curves recorded on the as-prepared MEA (3a) and on MEA worked for 460 h (3b). The results show that the long term operation leads to changes in MEA performance. Initially, the highest current densities were obtained on MEA with a standard (not sintered) cathode. The performance of MEA with cathode sintered at 320 °C was very similar, while for those treated at higher temperatures the obtained current densities were much lower. The worse performed MEA was the one with the cathode sintered at 360 °C.

However, after 460 hours of operation under constant current, the order in which the MEA performed changed. The standard electrode showed worse performance with degradation rate of 54.3μV. h⁻¹. The MEAs with the cathodes sintered at 320 °C and 340 °C reached current density of about 0.5 A cm⁻² at 0.5 V, while the calculated degradation rates (Table 1) showed much higher stability for the 340°C sintered cathode. The lowest performing MEA again was the one with the cathode sintered at 360 °C with degradation rate of 86.5 μV.h⁻¹. Obviously, the sintering at temperatures quite above the melting point of the binder, leads to decrease in the cell efficiency.

Figure 4 presents the evolution of *E/j* curves with service time of the best performing MEA (cathode sintered at 340 °C).

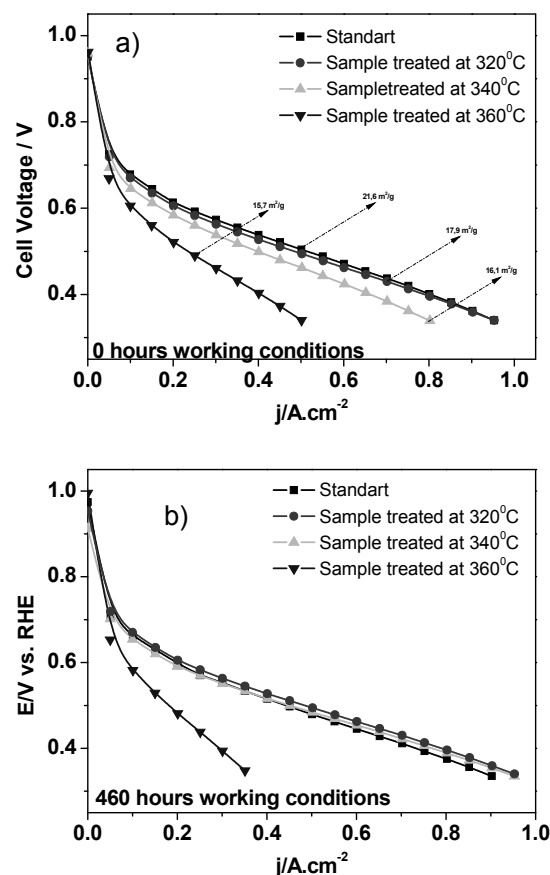


Fig. 3. *E/j* curves of MEA with cathodes sintered at varying temperatures; a) before durability tests; b) after 460 h of operation; scan rate 1 mVs⁻¹; cell temperature 160 °C.

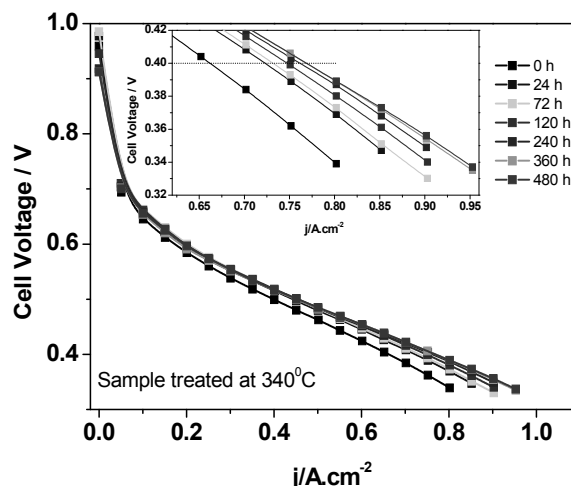


Fig. 4. *E/j* curves after different time of operation at 0.2 Acm⁻² at 160 °C of MEA with cathode sintered at 340 °C.

The performance is high without visible degradation. After the low drop of the current density observed in the low overpotential range during the first 72 h of operation, there was stabilization and even a slight improvement in the cell performance. The current density measured at

0.4V changed from 0.66A.cm⁻² in the beginning of the durability tests to 0.75 A.cm⁻² and 0.77 A.cm⁻² after 120 h and 480 h, respectively.

The break-in procedure used to characterize durability of the prepared MEA included also impedance measurements.

The Nyquist plots shown in Fig. 6 are typical for a PEMFC and contain three overlapped impedance semicircles corresponding to different electrochemical electrode processes. The diameter of the distinct loop is a measure for the respective

resistance [29]. Since the charge transfer resistance of the HOR is typically much smaller than the ORR one, the anode reaction HOR is only hinted at high frequencies (~10 kHz), while the cathode reaction (ORR) at middle frequency range (1kHz-1Hz), as well as mass transport at the lowest frequencies are well distinguished. The high-frequency intercept of the impedance with the real axis represents the total cell ohmic resistance, R_{el} , including resistances of the cables, electrodes and the electrolyte membrane (Fig. 5).

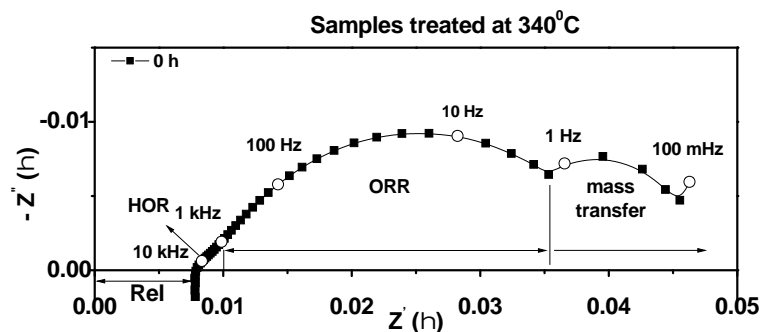


Fig. 5. Impedance curve of ORR in HT-PEFC single cell. Cell temperature 160 °C, stoichiometric factors Cathode/Anode = 2/2, gas temperature on both cameras 160 °C, current density 0.2A.cm⁻².

To analyze the possible changes on the anode side of the MEA, which could affect the cell performance, cyclic voltammetry was applied. The cathode compartment of the cell was shunted letting in an inert gas and the potential was scanned in the range -0.5V and 0.5V with scan rate of 50 mV s⁻¹. The results obtained are presented in Fig. 6. The CV curves do not change with time both in shape and current density, which is a proof for the anode stability and durability.

The Nyquist plots presented in Fig. 7 confirm the lack of MEA degradation. They show a reduction of R_{el} over the time (inset in Fig. 7) and facilitation of the mass transfer process. After the initial reduction of the ORR charge transfer resistance in the first 24 hours, it increases slightly, which could be explained with the Pt crystallites growth.

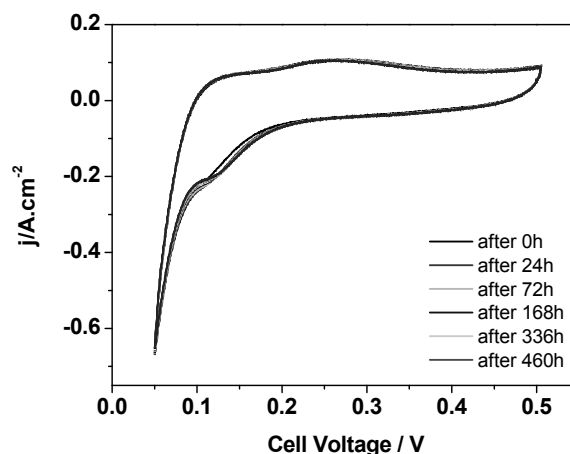


Fig. 6. CV curves on the anode side of the cell. Scan rate 50mv.s⁻¹, cell temperature 160 °C, stoichiometric factors Cathode/Anode = 2/2, range from 50mV to 500mV.

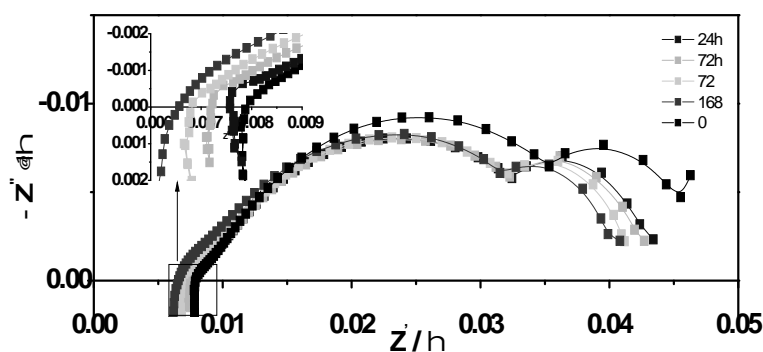


Fig. 7. Impedance curves of ORR in HT-PEFC single cell. Cell temperature 160 °C, stoichiometric factors Cathode/Anode = 2/2, gas temperature on both cameras 160 °C, current density 0.2 A.cm⁻².

In order to investigate the assumed Pt particle agglomeration in dependence of the treatment temperature and working time, the electrodes were analyzed by XRD. Fig 8(a) presents XRD patterns of all electrodes under study before the performed long term galvanostatic tests. The calculated values of the Pt particle size summarized in Table 2 show some increase of the crystallites size for the electrodes treated at 340 and 360 °C. This is not in accordance with the obtained data for the surface area of the electrodes (Table 1) and suggests that the registered decrease in the electrode specific surface area with the time of sintering is not only due to agglomeration of Pt crystallites, but is also related to the melting and degradation of the PTFE which lead to changes in the pores size and distribution and thus, to governing the transport phenomena of the cathode.

stronger the agglomeration of the Pt crystallites than the sintering temperature of electrode.

Table 2. Crystallite size calculated from XRD spectra by Scherer equation.

Sample	Temp. [°C]	time [h]	Cryst.size nm [111]
TT	standard	-	2.4
TT	320	-	2.4
TT	340	-	2.8
TT	360	-	2.8
cathode	standard	480	6.5
anode	standard	480	3.8
cathode	340	480	6.4
anode	340	480	3.6

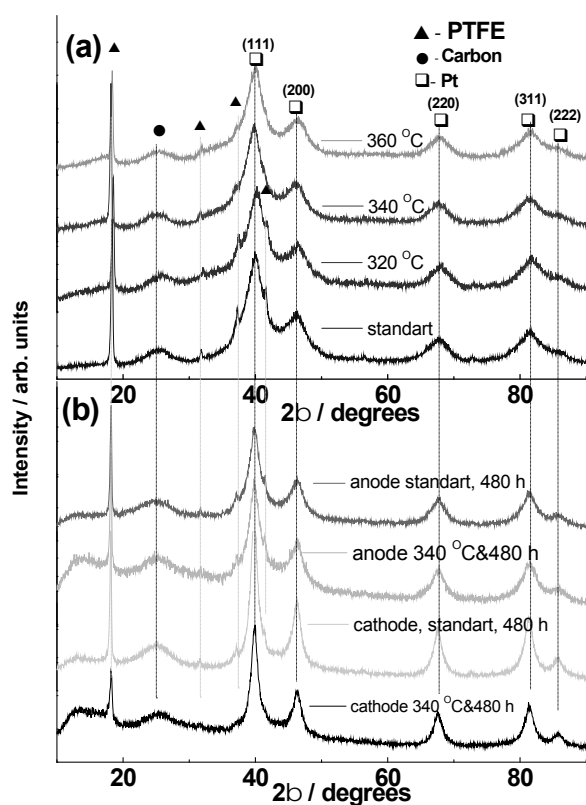


Fig.8. XRD patterns of the (a) as prepared electrodes and (b) after 480 h of operation in a MEA (as cathode or anode) at constant current of 0.5 A cm⁻².

In Figure 8(b) are presented XRD patterns of two electrodes (untreated and treated at 340°C) after 480 hours “in operando” mode. After the end of the long term test both investigated samples have similar particle size of about 6.4nm.

These results prove that the prolonged galvanostatic operation of the cathode affects much

CONCLUSIONS

The results obtained proved that the sintering procedure improves essentially the MEA durability. It is necessary only for the anode side where the produced water steam carry out partly phosphoric acid, which leads to degradation on the MEA performance. The registered changes in the GDE structure, porosity, as well as the established redistribution of the pores in the catalyst layer, prevent the leakage of the phosphoric acid from the membrane, thus avoiding loss of proton conductivity and degradation of the catalytic layer. It was found that the optimal temperatures for anode sintering is in the range 320 - 340 °C. Further increase of the sintering temperature leads to loses of electrochemical active surface area and decrease of the cell efficiency. The agglomeration process is influenced much more by working time rather than thermal treatment.

Acknowledgements: This research was supported by National Science Fund, Bulgaria, Contr. No. DTK – 02/02 and the German Academic Exchange Service (DAAD).

REFERENCES

1. Q. Li, J. Jensen, R. Savinell, N. Bjerrum, *Prog. Polym. Sci.*, **34**, 449, (2009).
2. Q. Li, R. He, J. Jensen, N. Bjerrum, *Fuel Cells*, **4**, 47, (2004).
3. L. Zhang, S. Chae, Z. Hendren, J. Park, M. Wiesner, *Chem. Eng. J.*, **204**, 87, (2012).
4. D. Boettner, M. Moran, *Energy*, **110**, 255, (2004).
5. P. Ghosh, U. Vasudeva, *Hydrogen Energy*, **36**, 3138, (2011).
6. A. Arsalis, A. Nielsen, S. Kær, *Hydrogen Energy*, **36**, 9815, (2011).

7. Q. Li, J. Jensen, R. Savinell, N. Bjerrum, *Polymer Science*, **34**, 449, (2009).
8. H. Tang, S. Wang, S. Jiang, M. Pan, *J. Power Sources*, **170**, 85, (2007).
9. T. Suzuki, S. Tsushima, S. Hirai, *Hydrogen Energy*, **36**, 12079 (2011).
10. S. Thanasilp, M. Hunsom, *Fuel cell*, **89**, 379 (2010).
11. J. Asensio, E. Sanchez, P. Gomez-Romero, *Chemical Society Reviews*, **39**, 3210, (2010).
12. S. Neophytidis, S. Zaafairatos, G. Papakonstantinou, J. Jaksic, F. Paloukis, *Int. J. Hydrogen Energy*, **30**, 393, (2005).
13. M. Min, J. Cho, K. Cho, H. Kim, *Electrochimica Acta*, **45**, 4211, (2000).
14. L. Xiong, A. Kannan, A. Manthiram, *Electrochemistry Communications*, **4**, 898 (2002).
15. S. Kraemer, M. Puchner, P. Jannasch, A. Lundblad, G. Lindbergh., Gas diffusion electrodes and membrane, **63**, 1856 (2008).
16. J. Lobato, P. Cañizares, M. Rodrigo, J. Linares, F. Pinar, *Journal of Hydrogen Energy*, **32**, 418 (2010).
17. C. Pan, Q. Li, J. Jensen, R. He, L. Cleemann, M. Nilsson, N. Bjerrum, Q. Zeng, *Journal of Power Sources*, **161**, 622 (2010).
18. A. Ong, G. Jung, C. Wu, W. M. Yan, *International Journal of Hydrogen Energy*, **18**, 249, (2010).
19. C. Wannek, W. Lehnert, J. Mergel, *Journal of Power Sources*, **192**, 258, (2009).
20. M. Mamlouk, K. Scott, *International Journal of Energy Research*, **35**, 507, (2011).
21. Y. Oono, A. Sounai, M. Hori, *Journal of Power Sources*, **210**, 366, (2012).
22. Y. Oono, T. Fukuda, A. Sounai, M. Hori, *Journal of Power Sources*, **1/5**, 95, (2009).
23. B. Tripathi, M. Kumar, V. Shahi, *Journal of Membrane Science*, **340**, 52, (2009).
24. A. Modestov, M. Tarasevich, V. Filimonov, N. Zagudaeva, M. Kim, G. Jeong, K. Eom, E. Cho, J. Ryu, H. Kim, H. Kwon, *Journal of Advanced Functional Materials*, **9**, 367, (2006).
25. A. Majerus, F. Conti, C. Korte, W. Lehnert, D. Stoltena, *Electrochimica Acta*, **52/2**, 1155, (2012).
26. J. Lanford, A. Wilson, *Appl. Crystallogr.*, **33**, 964, (1978).
27. J. Lanford, A. Wilson, *Applied Crystallography*, **11**, 102, (1978).
28. P. Rae, D. Dattelbaum, *Polymer*, **45**, 7367, (2004).
29. X. Yuan, H. Wang, J. Sun, J. Zhang, *International Journal of Hydrogen Energy*, **34**, 1108, (2007).

